Tuning nanotubular structures by templateless electropolymerization with thieno[3,4-b]thiophene-based monomers with different substituents and water content

Maroua Khodja, Mejda El Kateb, Mohammed Beji, Frédéric Guittard,
Thierry Darmanin

Tuning nanotubular structures by templateless electropolymerization with thieno[3,4-*b*]thiophene-based monomers with different substituents and water content

Maroua Khodja[a], Mejda El Kateb[a], Mohammed Beji[a], Frédéric Guittard[b,c] and Thierry Darmanin[b,*]

[a]University of Tunis El Manar, Laboratory of Structural Organic Chemistry, Faculty of Sciences of Tunis, 2092 Tunis, Tunisia

[b]Université Côte d'Azur, NICE Lab, 06200 Nice, France.

Corresponding author: thierry.darmanin@unice.fr

[c]University California Riverside, Department of Bioengineering, Riverside, CA, USA

Abstract

Here, templateless electropolymerization is employed to produce nanotubular structures from various thieno[3,4-*b*]thiophene-based monomers that differ in substituent structure and size, as well as the linker connecting the thieno[3,4-*b*]thiophene core and substituent. The formation densely packed vertically aligned are obtained from monomers with a pyrene substituent and when a significant amount of water ($CH_2Cl_2 + H_2O$) is included in the solvent. The geometrical parameters of the nanotubes are highly dependent on the electopolymerization method. A significant amount of air is trapped within the structure of the densely packed open nanotubes obtained with $Q_s = 100$ mC cm^{-2} causing an increase in water contact angle (θ_w) up to 82.6° (intermediate state between the Wenzel and the Cassie-Baxter state), and θ_w can become even more hydrophobic by further modifying the deposition method or the electrolyte.

Keywords: Nanotubes, Nanostructures, Electrochemistry, Conducting polymers, Wettability.

1. Introduction

The design of well-defined nanoporous surfaces such as vertically aligned nanotubes has many applications in encapsulation, drug delivery, biomedical imaging, catalysis, electrocatalysis, photocatalysis, batteries, supercapacitors, photovoltaics and sensors [1–7]. The control of their dimensions (diameter, height, porosity) and shape are fundamental to fully understand the relationship between geometrical parameters of the nanostructures and observed surface properties, such as surface wettability [8–13]. For example, any trapped air within nanotubes can significantly impact surface hydrophobicity, as predicted by the Cassie-Baxter equation.

One of the most commonly employed methods to produce ordered nanostructures is through hard membranes such as anodized aluminum oxide (AAO). With this approach, well ordered vertically aligned nanotubes can be prepared, however this method is difficult and time-consuming, and furthermore different membranes are necessary for each modification of nanotube parameter (diameter, height, etc.) [14–18]. Templateless electropolymerization is an excellent alternative that allows rapid production of homogenous nanoporous structures on a substrate. The substrate used for electropolymerization has to be conductive and not easily oxidizable such as gold, platinum or stainless steel but also a thin conductive layer can be added on a non-conductive substrate. An example is transparent glass substrates covered by indium-tin oxide (ITO). Substrates of complex geometry such as meshes or micro-patterned substrates can be also used even if a textures can affect the polymer growth [19–22]. Moreover, it should also be worth-noting that other strategies were employed in the literature on conductive substrate to tune the surface roughness/wettability including chemical etching [23], surface oxidation [24], and anodization [25], but electropolymerization seems to be one of the more versatile process.

With this process, tubular structures form around gas bubbles that are produced *in-situ* during electropolymerization. Templateless electropolymerization of pyrrole in water (H_2O) has been extensively studied in the literature [26–35] and different gases (O_2 and/or H_2) are produced from H_2O during this reaction. The extent to which this occurs depends on the electropolymerization process, and a surfactant is necessary to stabilize the gas bubbles and induce polymer growth around them. Two main strategies in this area have been reported. First, using sulfonic acids and conducting the electropolymerization via cyclic voltammetry, H_2 bubbles formed from H^+ ($2\,H^+ + 2\,e^- \rightarrow H_2$) released from sulfonic acids during the back

scans [26–28]. With this mechanism, tubular structures and cups of very large porosity were reported as a function of the potential range as well as the scan rate. Margaritondo et al. investigated the microcontainer shape from the electropoymerization of pyrrole on H_2 bubbles using real-time microradiography and observed the existence of a deformation force at the three-phase boundary changing from spherical to elliptical and then to cylindrical [29]. By contrast, the group of Debiemme-Chouvy observed the formation of polypyrrole nanowires without strong acid but in the presence of anions of weak acid such as monohydrogenophosphate and non-acidic anions (perchlorate) [31–35]. In this case, at constant potential, the authors noted the release of O_2 bubbles from H_2O ($2\,H_2O \rightarrow O_2 + 4\,H^+ + 4\,e^-$).

Unfortunately, electropolymerization in H_2O often requires high monomer concentration and most of the monomers employed have limited solubility in H_2O. Fortunately, the possibility to use organic solvent such as dichloromethane (CH_2Cl_2) with trace H_2O present in solution was recently reported [36–42]. By designing monomers that can also play the role of the surfactant, it is possible to obtain homogeneous porous structures without a separate surfactant. Exceptional results such as vertically aligned nanotubes with strong water adhesion were reported with monomers derived from 3,4-phenylenedioxythiophene (PheDOT), 3,4-naphtalenedioxythiophene (NaphDOT) and thienothiophene [36–39]. Moreover, it was determined that the rigidity of the polymer is a key parameter for this self-assembly. For example, exceptionally strong effect of small structural variations (2-naphtylmethyl-, 1-naphtylmethyl-) in functionalized PheDOT was observed from uni-directional growth (1D) of vertically aligned nanotubes for 2Na-PheDOT to ribbon-like nanostructures (2D) for 1Na-PheDOT [36].

Among these promising monomers, thieno[3,4-*b*]thiophene derivatives combine both exceptional opto-electronic properties and exceptional capacity to form nanoporous structures including nanotubes, nanocups and hollow spheres [40–42]. Here, we study a series of original thieno[3,4-*b*]thiophene monomers with ester and thioester groups directly bound on the 2-position. As shown on Scheme 1, different substituents including fluorinated chains, alkyl chains and very different aromatic groups are tested. In order to better determine the influence of H_2O content on the formation of nanoporous structures, two different solvents are investigated: CH_2Cl_2 and CH_2Cl_2 saturated with H_2O ($CH_2Cl_2 + H_2O$).
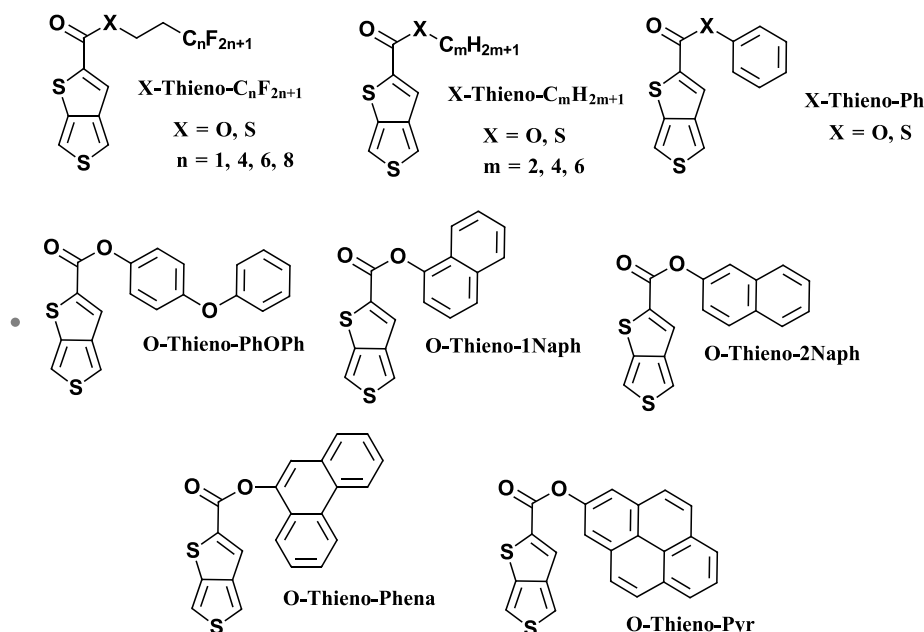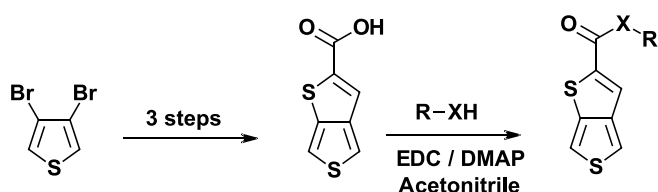
Scheme 1. Original monomers investigated in this work.

2. Materials and method

2.1 Monomer synthesis

Thieno[3,4-*b*]thiophene-2-carboxylic acid was synthesized in three steps from 3,4-dibromothiophene using a procedure reported in the literature [43–45].

Scheme 2. Synthesis strategy for the monomers.

Thieno[3,4-*b*]thiophene-2-carboxylic acid. Yield 64%; White powder; δ_H (400 MHz, DMSO-d$_6$): 7.99 (dd, J = 2.9 Hz, J = 0.5 Hz, 1H), 7.74 (m, 2H); δ_C (400 MHz, DMSO-d6): 163.96, 145.65, 140.28, 138.54, 123.56, 118.36, 112.72.

For the monomer synthesis, 1 eq. of thieno[3,4-*b*]thiophene-2-carboxylic acid was mixed with 1.5 eq. of *N*-(3-dimethylaminopropyl)-*N'*-ethylcarbodiimide hydrochloride (EDC) and a catalytic amount of 4-(dimethylamino)pyridine (DMAP) in 20 mL of absolute acetonitrile. After stirring for 30 min, 1.5 eq. of the corresponding alcohol or thiol was added to the

mixture. After one day, the crude product was purified by column chromatography on silica gel (eluent: cyclohexane/diethyl ether 50:10). The monomer characterization data can be found in ESI.

2.2 Electropolymerization

All electropolymerizations were performed with an Autolab potentiostat (from Metrohm). Three electrodes were used: a 2 cm^2 gold-coated silicon wafer as working electrode (from Neyco), a carbon rod as counter-electrode (from Metrohm) and a saturated calomel electrode (SCE) as the reference electrode (from Hach Lange). 10 mL of a solution containing 0.1 M of tetrabutylammonium perchlorate (Bu$_4$NClO$_4$) as supporting electrolyte and 0.01 M of monomer was inserted into an electrochemical cell. In order to study the influence of H$_2$O content on the formation of H$_2$/O$_2$ gas bubbles, two solvents were used: dichloromethane (CH$_2$Cl$_2$) or CH$_2$Cl$_2$ saturated with H$_2$O (CH$_2$Cl$_2$ + H$_2$O). CH$_2$Cl$_2$ + H$_2$O was prepared by mixing CH$_2$Cl$_2$ with a high amount of H$_2$O and removing any excess H$_2$O by extraction after decantation. Templateless electropolymerizations were performed via cyclic voltammetry from -1 V to the monomer oxidation potential (here, E^{ox} ≈ 1.65–1.75 V vs SCE), at a scan rate of 20 mV s^{-1}, for 1, 3 or 5 scans.

2.3 Surface characterization

The surface structures were characterized by scanning electron microscopy (SEM) with a 6700F microscope (JEOL). For the surface wettability, a DSA30 goniometer (from Bruker) was used with 2 μL liquid droplets. The apparent contact angles (θ) were taken at the triple point. Three liquids were used: water (γ_L = 72.8 mN/m), diiodomethane (γ_L = 50.0 mN/m) and hexadecane (γ_L = 27.6 mN/m). Five measurements were performed for each data point.

3. Result and Discussion

3.1. Templateless electropolymerization

Here, in order to determine the influence of H$_2$O content, templateless electropolymerizations were performed with two solvents: neat dichloromethane (CH$_2$Cl$_2$) and dichloromethane saturated with water (CH$_2$Cl$_2$ + H$_2$O). The cyclic voltammograms of the two solvents with 0.1 M of Bu$_4$NClO$_4$ and without any monomer are clearly quite different (Figure 1). First, a large

peak at $\approx$ -0.5 V *vs* SCE is present during the back scan in CH_2Cl_2 + H_2O, confirming the reaction $2\ H_2O + 2\ e^- \rightarrow \mathbf{H_2}$ (bubbles) + 2 OH⁻. The peak starts at $\approx$ 0.0 V extends to $\approx$ -0.85 V. For the reaction $2\ H_2O \rightarrow \mathbf{O_2}$ (bubbles) + 4 H⁺ + 4 e⁻, a peak is present during the forward scan but rather from $\approx$ 2.0 V *vs* SCE.
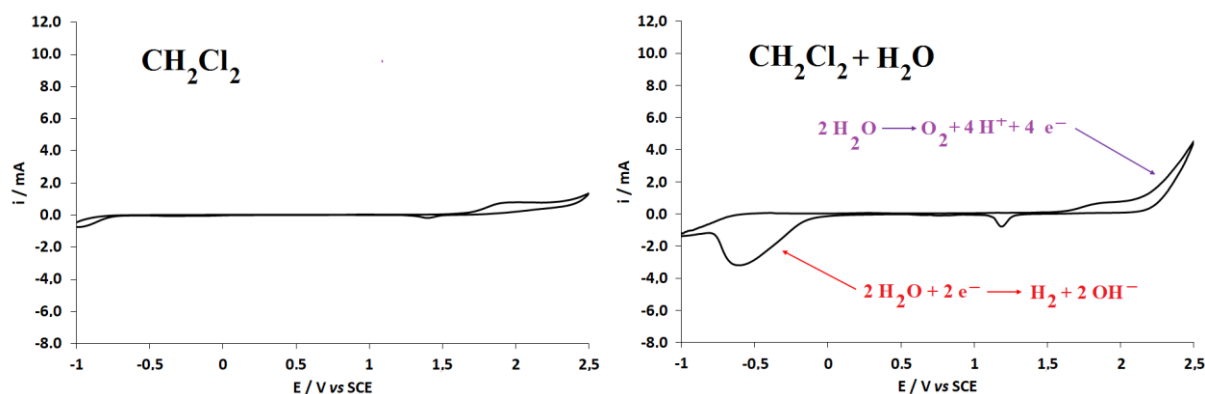
Figure 1. Cyclic voltammograms of CH_2Cl_2 (on the left) and CH_2Cl_2 + H_2O (on the right) with Bu_4NClO_4 (0.1 M) as supporting electrolyte. 1 scan at 20 mV s⁻¹.

After adding the monomers to the electrochemical cell, their oxidation potential was found to be E^{ox} = 1.65-1.75 V *vs* SCE depending on the substituent structure. Therefore, in the potential range explored here, the formation of H_2 bubbles is expected for electrodepositions via cyclic voltammetry. Therefore, electrodepositions via cyclic voltammetry were performed with each monomer from -1 V to E^{ox}, and different numbers of scans (1, 3, 5) were explored to investigate polymer growth. Examples of cyclic voltammograms after 5 scans are given in Figure 2. The oxidation and reduction of the electrodeposited conducting polymers is evident on all these voltammograms. With CH_2Cl_2 + H_2O as solvent, a large peak at $\approx$ -0.5 V *vs* SCE is also often observed, corresponding to the reaction $2\ H_2O + 2\ e^- \rightarrow \mathbf{H_2}$ (bubbles) + 2 OH⁻. In these cases, the polymer films were removed from the substrate by these gas bubbles.
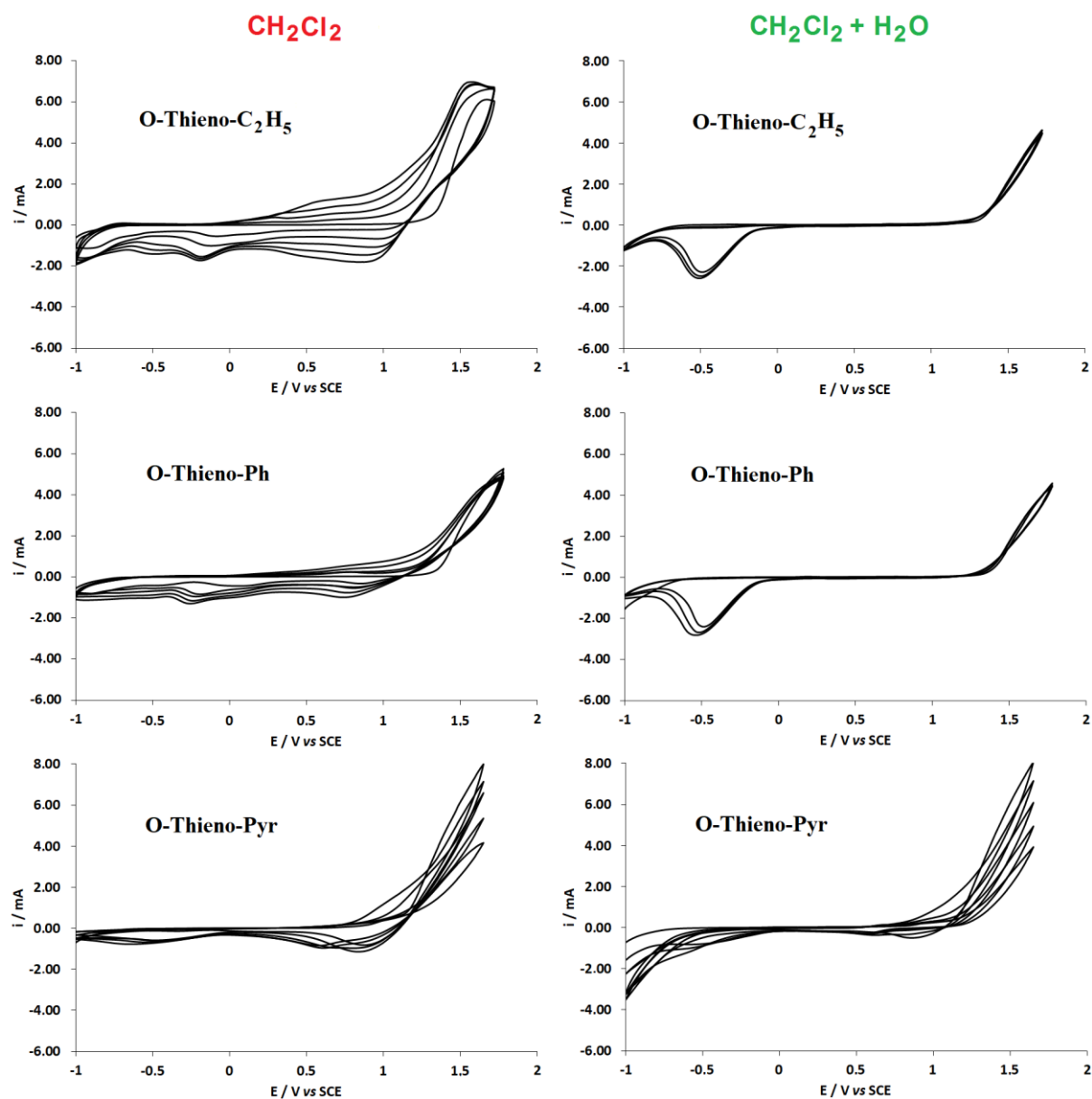
Figure 2. Cyclic voltammograms of O-Thieno-C_2H_5, O-Thieno-Ph and O-Thieno-Pyr in CH_2Cl_2 (on the left) and CH_2Cl_2 + H_2O (on the right) with Bu_4NClO_4 (0.1 M) as supporting electrolyte. 5 scans at 20 mV s^{-1}.

3.2. Formation of nanoporous structures

Initially, CH_2Cl_2 was tested as electropolymerization solvent because it has been shown that by using well-designed monomers it is possible to obtain nanoporous structures, even with trace H_2O. Example SEM images after 3 deposition scans are highlighted in Figures 3-6. Using the fluorinated monomers O-Thieno-C_nF_{2n+1}, it was observed that the surface

morphology transitioned from nanofibrous structures to spherical structures as the fluorinated chain length increased (Figure 3). This is due to an increase in polymer insolubility. With very long fluorinated chains (O-Thieno-C_8F_{17}), the surface is relatively smooth because the steric hindrance induced by these long chain substituents becomes very significant. The same tendency is observed with the sulfur analogues (S-Thieno-C_nF_{2n+1}) even though an increase in polymer solubility in CH_2Cl_2 is expected with the presence of sulfur atoms (ESI, Figure S1). The influence of side change length is more sensitive with alkyl chains, as spherical nanoparticles are obtained but only from very short alkyl chains (O-Thieno-C_2H_5 and S-Thieno-C_2H_5) (ESI, Figure 2). For the same reason, the polymers formed with S-Thieno-C_4H_9 and S-Thieno-C_6H_{13} were completely soluble in CH_2Cl_2 and polymer films could not be electrodeposited using these monomers. For the monomers with aromatic substituents, relatively smooth surfaces are obtained except with Thieno-Pyr which leads to spherical particles (ESI, Figure 3). Hence, for all the monomers tested here in CH_2Cl_2, the presence of porous structures was not clearly observed.
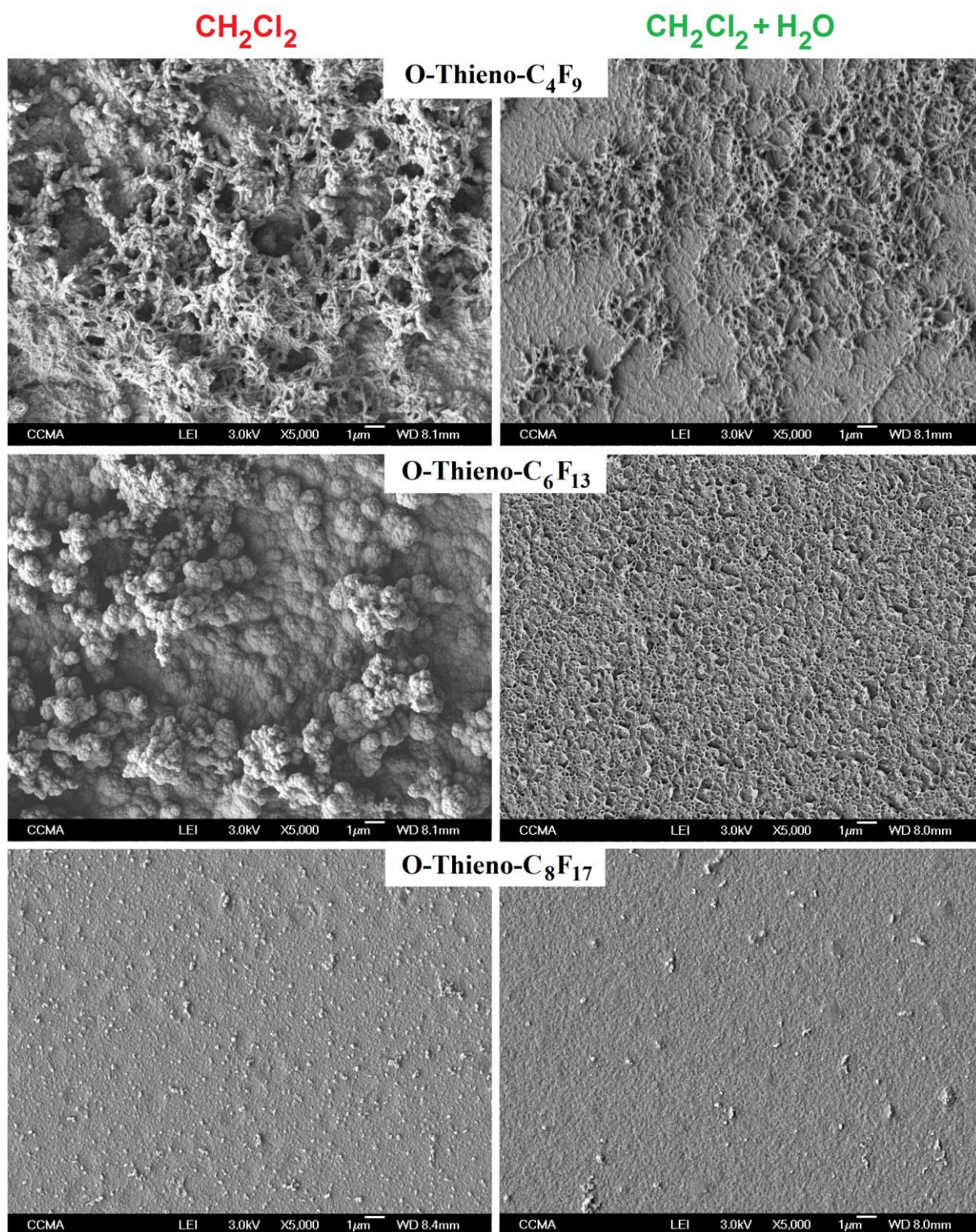
Figure 3. SEM images of O-Thieno-C$_4$F$_9$, O-Thieno-C$_6$F$_{13}$ and O-Thieno-C$_8$F$_{17}$ electropolymerized in CH$_2$Cl$_2$ (on the left) and CH$_2$Cl$_2$ + H$_2$O (on the right) with Bu$_4$NClO$_4$ (0.1 M) as supporting electrolyte. Cyclic voltammetry with 3 scans at 20 mV s^{-1}.

Moreover, the study of their surface wettability (ESI, Table S1) reveals the higher hydrophobicity with θ_w up to 157.9° for the surface obtained from S-Thieno-C_6F_{13} and S-Thieno-C_4F_9 due to the low surface energy (fluorinated chains) and surface structures (spherical particles or nanofibers). Films obtained from monomers with short alkyl chains (O-Thieno-C_2H_5 and S-Thieno-C_2H_5) are also highly hydrophobic due to the presence of spherical particles and large wrinkles.

Films were also prepared in CH_2Cl_2 + H_2O to determine the influence of H_2O content (ESI, Table S2). For the fluorinated monomers, the films are similar to than obtained in CH_2Cl_2 except than the films are slightly less structured. Nanoporosity is clearly observed, but only with O-Thieno-C_6F_{13} as monomer indicating than the presence of nanoporosity is highly dependent on the substituent nature. This confirms previous works showing that the polymer needs to be very rigid in order to stabilize gas bubbles released during electropolymerization (perfluorinated chains are more rigid than hydrocarbon chains and their rigidity increases with chain length). Moreover, with all the very short fluorinated chains (CF_3) and all the studied hydrocarbon chains (C_2H_5, C_4H_9 and C_6H_{13}), it is observed that the polymer films are removed from the substrate by gas bubbles as the release of such a significant amount of gas imposes significant pressure on the polymer coating. This is also the case for all the aromatic-substituted monomers, except Thieno-Pyr for which this phenomenon was much less drastic. With these aromatic groups, we also attempted deposition with a 50% reduction in H_2O content. With this strategy, polymer films were only obtained from O-Thieno-Ph and O-Thieno-2Naph (Figure 4), but the films display small nanotubular structures.

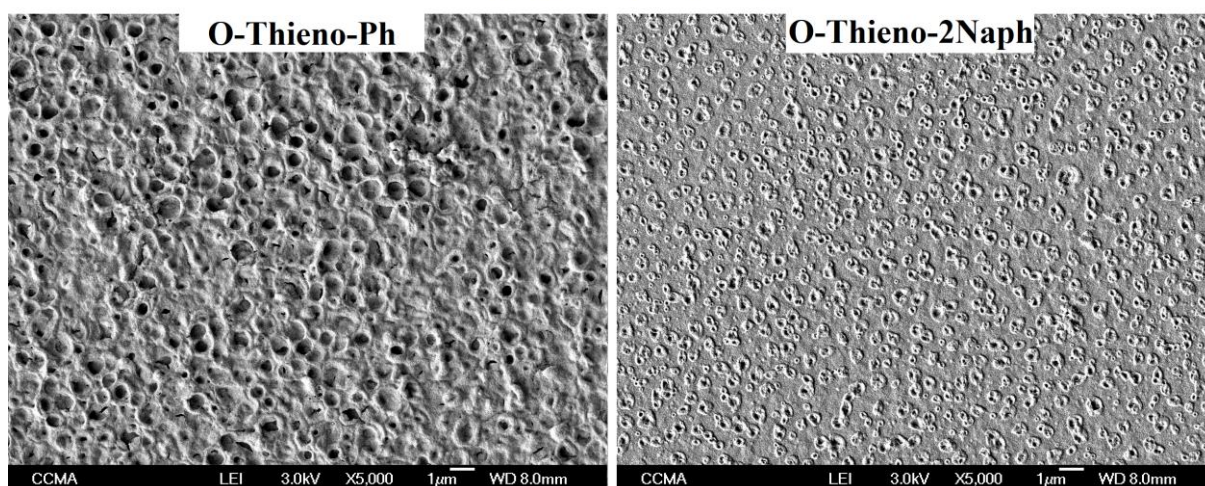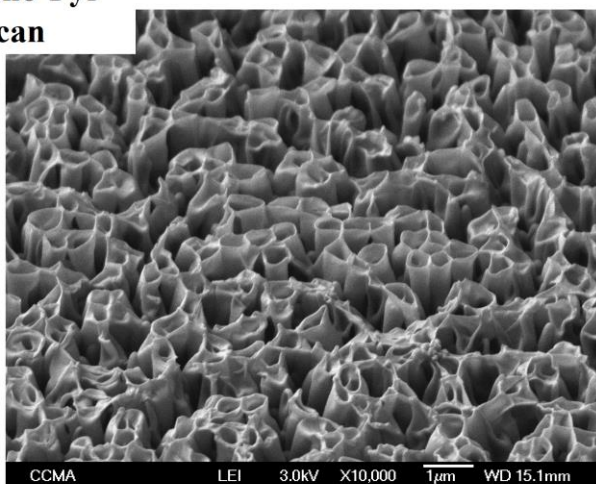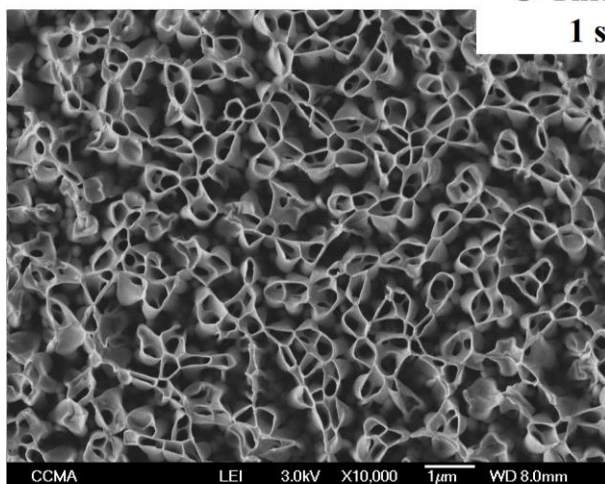**Figure 4.** SEM images of O-Thieno-Ph and O-Thieno-2-Naph electropolymerized in CH_2Cl_2 + H_2O (50%) with Bu_4NClO_4 (0.1 M) as supporting electrolyte. Cyclic voltammetry with 3 scans at 20 mV s^{-1}.

In the case of Thieno-Pyr, pyrene participates readily with the polymerization (it has an oxidation potential close to that of thieno[3,4-*b*]thiophene) while also simultaneously inducing high π-stacking interactions. As shown in Figure 5, the capacity of Thieno-Pyr to form very large tubular structures in CH_2Cl_2 + H_2O is impressive, especially compared to all the other monomers, demonstrating also the importance of H_2O content. After just 1 scan, densely packed, vertically aligned nanotubes with a diameter of roughly 500 nm and height > 1 μm are observed on the surface (Figure 6). This indicates that the polymer growth around the gas bubbles is uni-dimensional (1D-growth). However, as the number of scans increases a significant increase in both nanotube diameter and length is observed.
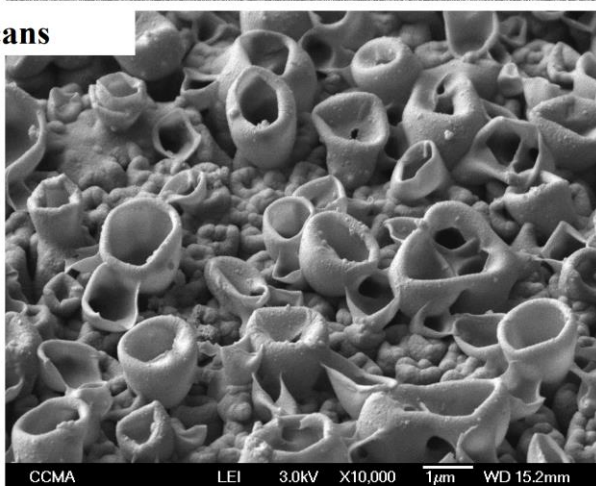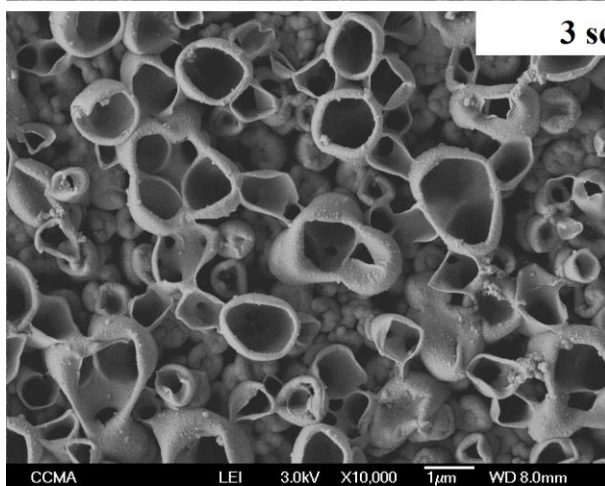
$CH_2Cl_2 + H_2O$
O-Thieno-Pyr
1 scan

CCMA   LEI   3.0kV   X10,000   1μm   WD 8.0mm

CCMA   LEI   3.0kV   X10,000   1μm   WD 15.1mm

3 scans

CCMA   LEI   3.0kV   X10,000   1μm   WD 8.0mm

CCMA   LEI   3.0kV   X10,000   1μm   WD 15.2mm

5 scans

CCMA   LEI   3.0kV   X10,000   1μm   WD 8.0mm

CCMA   LEI   3.0kV   X10,000   1μm   WD 15.2mm

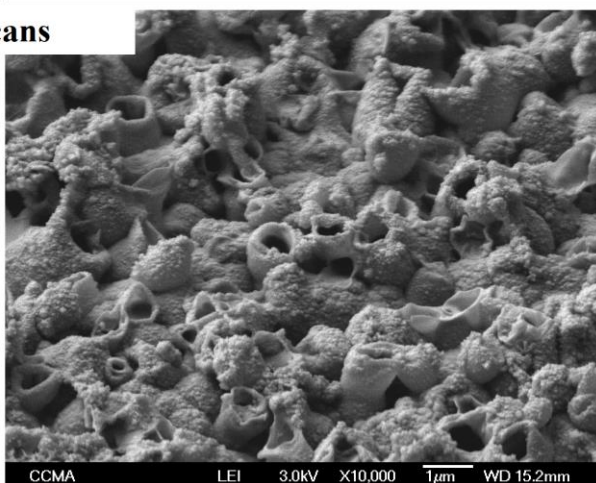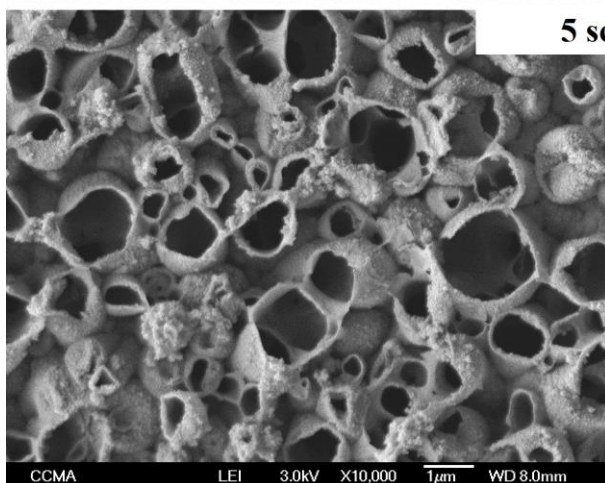**Figure 5.** SEM images of O-Thieno-Pyr electropolymerized in CH_2Cl_2 + H_2O with Bu_4NClO_4 (0.1 M) as supporting electrolyte. Cyclic voltammetry with 1, 3 and 5 scans at 20 mV s^{-1}. The pictures are taken without (on the left) and with surface inclination of 45°.
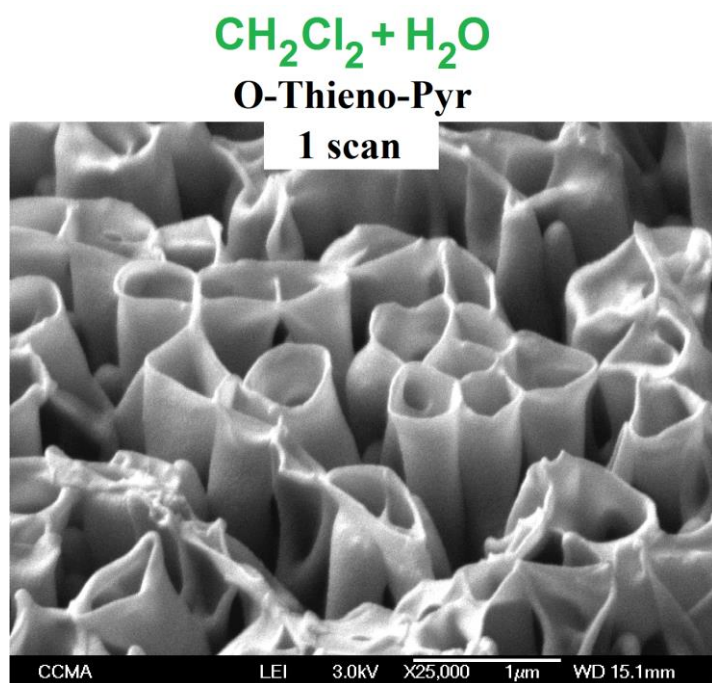

Figure 6. SEM images of O-Thieno-Pyr electropolymerized in CH_2Cl_2 + H_2O with Bu_4NClO_4 (0.1 M) as supporting electrolyte. Cyclic voltammetry with 1 scan at 20 mV s^{-1}. The pictures are taken with high magnification and with surface inclination of 45°.

Table 1. Roughness (R_a and R_q) and wettability data for the polymer films obtained from Thieno-Pyr in Bu_4NClO_4/ CH_2Cl_2 + H_2O and as a function of the deposition method.

| Deposition method	R_a [nm]	R_q [nm]	θ_w [deg]	θ_{diiodo} [deg]	θ_{hexa} [deg]
CV (1 scan)	244 ± 25	316 ± 33	109.0 ± 4.4	24.5 ± 0.3	0
CV (3 scans)	*	*	104.0 ± 7.2	31.1 ± 0.9	0
CV (5 scans)	*	*	103.0 ± 6.0	25.4 ± 5.5	0
CP (12.5 mC cm^{-2})	38 ± 4	48 ± 5	79.7 ± 4.2	0	0
CP (25 mC cm^{-2})	36 ± 4	42 ± 6	68.2 ± 3.7	0	0
CP (50 mC cm^{-2})	32 ± 6	42 ± 7	59.4 ± 3.8	0	0
CP (100 mC cm^{-2})	89 ± 8	122 ± 9	82.6 ± 5.9	0	0
CP (200 mC cm^{-2})	*	*	55.2 ± 2.8	0	0
CP (400 mC cm^{-2})	*	*	49.6 ± 7.9	0	0

*too rough for the apparatus

Thieno-Pyr was also electropolymerized at constant potential and using different deposition charges (Qs from 12.5 to 400 mC cm^{-2}). At low Qs, densely packed nanotubes of very low diameter and height ($\approx$ 50 nm) formed (Figure 7). However, as Qs increased the nanotube height increases in size much more than the diameter. This is expected because at constant potential only O_2 gas is formed while by cyclic voltammetry both O_2 and H_2 are released. Here, the formation of extremely long nanotubes is possible because the polymer growth is only 1D. For example, the nanotube diameter and length are $\approx$ 500 nm and 5 μm for Qs = 200 mC cm^{-2} and $\approx$ 1 μm and 10 μm for Qs = 400 mC cm^{-2}. The surface hydrophobicity can increase or decrease as a function of Qs, and higher surface hydrophobicity with θ_w = 82.6° is obtained for Qs = 100 mC cm^{-2} (Table 1). Even if the polymer is intrinsically hydrophilic, these results can be explained using the Cassie-Baxter equation if air is trapped inside the surface roughness [46]. The densely packed open nanotubes obtained for Qs = 100 mC cm^{-2} permit trapping of a significant quantity of air, increasing θ_w to 82.6°.
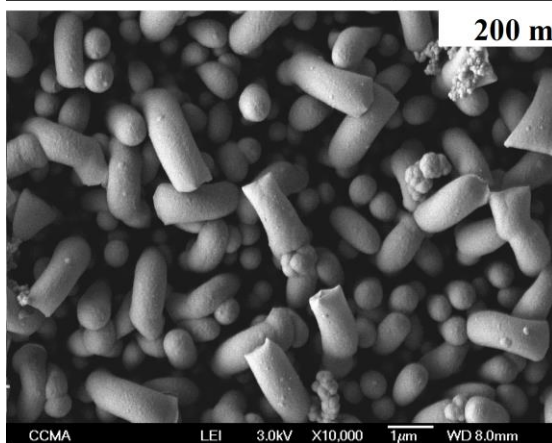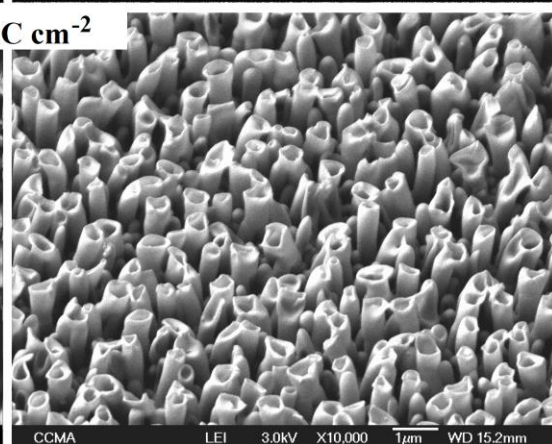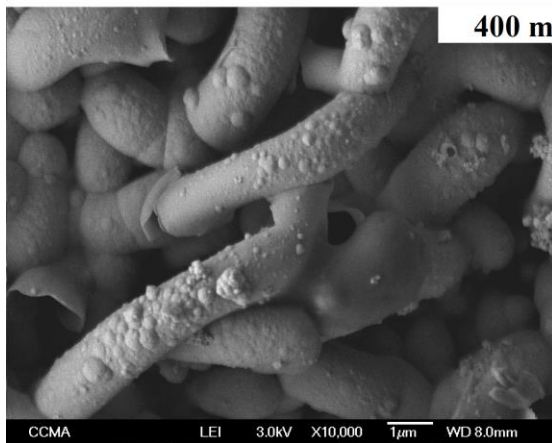
CH$_2$Cl$_2$ + H$_2$O
O-Thieno-Pyr
50 mC cm^{-2}
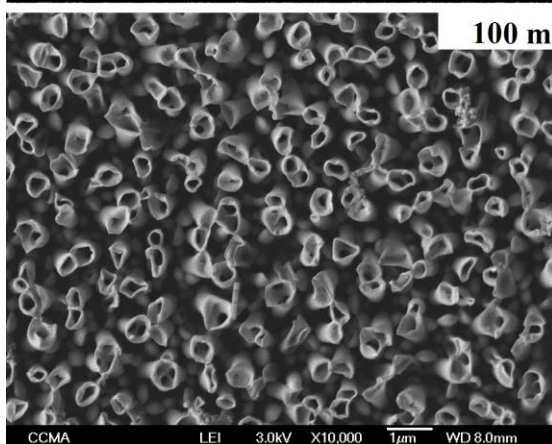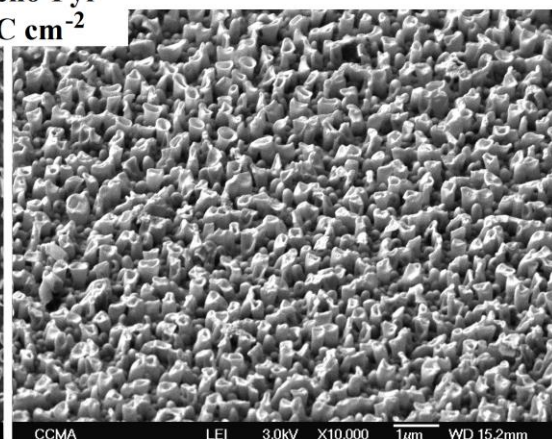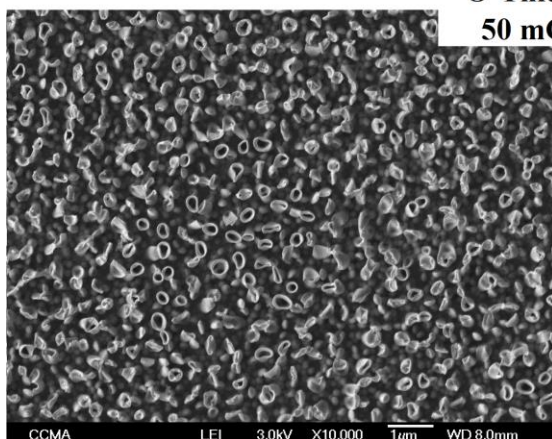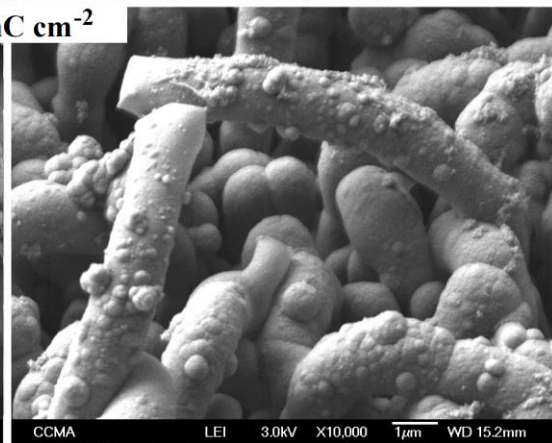

100 mC cm^{-2}

200 mC cm^{-2}
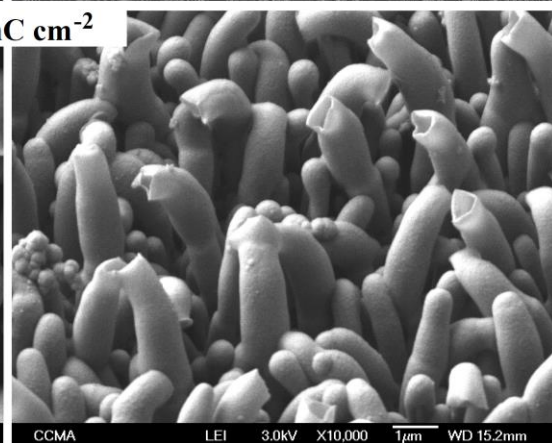
400 mC cm^{-2}

Figure 7. SEM images of O-Thieno-Pyr electropolymerized in CH_2Cl_2 + H_2O with Bu_4NClO_4 (0.1 M) as supporting electrolyte. Constant potential with Qs = 50, 100, 200 and 400 mC cm^{-2}. The pictures are taken without (on the left) and with surface inclination of 45°.

Two additional classical electrolytes were also tested: Bu_4NBF_4 and Bu_4NPF_6. Relatively similar structures are obtained from these electrolytes as shown in ESI, Figures S4-S5 and Table S3. It is noted that the surfaces obtained with Bu_4NBF_4 are more hydrophobic (θ_w up to 130.8°).

4. Conclusion

The templateless electropolymerization [26] is a unique method to rapidly form ordered nanotubular structures with unique wetting properties. In this work, we have shown that combining thieno[3,4-*b*]thiophene monomer with pyrene substituent allows producing densely packed vertically aligned nanotubes if a significant amount of water (CH_2Cl_2 + H_2O) is present is the solvent. For example, densely packed, open nanotubes obtained for Qs = 100 mC cm^{-2} allowed trapping of a high amount of air and thus increased the water contact angle (θ_w) up to 82.6° (intermediate state between the Wenzel and the Cassie-Baxter state) and could become even more hydrophobic by further modifying the deposition method or the electrolyte. Such materials could be used in the future in many applications and especially in water-harvesting systems with a bioinspiration from cactus spines [47], systems with high adhesion forces such as gecko pads [48,49], as well as applications in oil/water separation membranes [50,51].

5. Acknowledgment

References

[1] A.J. Clancy, M.K. Bayazit, S.A. Hodge, N.T. Skipper, C.A. Howard, M.S.P. Shaffer, Chem. Rev. 118 (2018) 7363–7408.

[2] Y. Zhang, Z. Jiang, J. Huang, L. Y. Lim, W. Li, J. Deng, D. Gong, Y. Tang, Y. Lai, Z. Chen, RSC Adv. 5 (2015) 79479–79510.

[3] A.C. Dillon, Chem. Rev. 110 (2010) 6856–6872.

[4] P. Král, B. Wang, Chem. Rev. 113 (2013) 3372–3390.

[5] M. Salavati-Niasari, F. Davar, M. Bazarganipour, Dalton Trans. 39 (2010) 7330–7337.

[6] J. Meng, S. Wang, Adv. Mater. DOI: 10.1002/adfm.201904796.

[7] G. Yang, H. Huang, J. Chen, D. Gan, F. Deng, Q. Huang, Y. Wen, M. Liu, X. Zhang, Y. Wei, J. Mol. Liq. (2019) 111874.

[8] Z. Cheng, J. Gao, L. Jiang, Langmuir 26 (2010) 8233–8238.

[9] L. Ge, S. Sethi, L. Ci, P.M. Ajayan, A. Dhinojwala, Proc. Natl. Acad. Sci. U. S. A. 104 (2007) 10792–10795.

[10] Y. Lai, X. Gao, H. Zhuang, J. Huang, C. Lin, L. Jiang, Adv. Mater. 21 (2009) 3799–3803.

[11] Q. Li, D. Wu, Z. Guo, Soft Matter 15 (2019) 6803–6810.

[12] Z. Sun, T. Liao, K. Liu, L. Jiang, J. H. Kim, S. X. Dou, Small 10 (2014) 3001–3006.

[13] K. Zhang, S. Huang, J. Wang, G. Liu, Angew. Chem. Int. Ed. 58 (2019) 12004–12009.

[14] D. Wu, D. Zhang, Y. Ye, L. Ma, B. Minhas, B. Liu, H. A. Terryn, J.M.C. Mol, X. Li, Chem. Eng. J. 368 (2019) 138–147.

[15] J. Yu, S. Xiang, M. Ge, Z. Zhang, J. Huang, Y. Tang, L. Sun, C. Lin, Y. Lai, Coatings 8 (2018) 374.

[16] M. Paulose, H.E. Prakasam, O.K. Varghese, L. Peng, K.C. Popat, G.K. Mor, T.A. Desai, C.A. Grimes, J. Phys. Chem. C 111 (2007) 14992–14997.

[17] L. Lee, S.J. Park, Chem. Rev. 114 (2014) 7487–7556.

[18] H.-A. Lin, S.-C. Luo, B. Zhu, C. Chen, Y. Yamashita, H.-h. Yu, Adv. Funct. Mater. 23 (2013) 3212–3219.

[19] G. Ramos Chagas, C. Fradin, F. Celestini, F. Guittard, T. Darmanin, ChemPhysChem 20 (2019) 1905–1905.

[20] T. Darmanin, F. Guittard, Nano-Struct. Nano-Objects 7 (2016) 64–68.

[21] B. Bombera, G. Ramos Chagas, A. Valsesia, P. Colpo, F. Guittard, T. Darmanin, ChemNanoMat 5 (2019) 1239–1243.

[22] T. Darmanin, R. Bombera, P. Colpo, A. Valsesia, J.-P. Laugier, F. Rossi, F. Guittard, ChemPlusChem 82 (2017) 352–357.

[23] S. Peng, B. Bhushan, J. Colloid Interface Sci. 461 (2016) 273–284.

[24] K. Li, J. Zhang, J. Chen, G. Meng, Y. Ding, Z. Dai, ACS Appl. Mater. Interfaces, 8 (2016)

10005–10013.

[25] S. Zhang, J. Huang, Y. Tang, S. Li, M. Ge, Z. Chen, K. Zhang, Y. Lai, Small, 13 (2017) 1600687.

[26] L. Qu, G. Shi, F. Chen, J. Zhang, Macromolecules 36 (2003) 1063−1067.

[27] J. Yuan, L. Qu, D. Zhang, G. Shi, Chem. Commun. 0 (2004) 994−995.

[28] L. Qu, G. Shi, J. Yuan, G. Han, F. Chen, J. Electroanal. Chem. 561 (2004) 149–156.

[29] J.T. Kim, S.K. Seol, J. H. Je, Y. Hwu, G. Margaritondo, Appl. Phys. Lett. 94 (2009) 034103.

[30] B. Parakhonskiy, D. Shchukin, Langmuir 31 (2015) 9214−9218.

[31] C. Debiemme-Chouvy, Electrochem. Solid-State Lett. 10 (2007) E24−E26.

[32] C. Debiemme-Chouvy, A. Fakhry, F. Pillier, Electrochim. Acta 268 (2018) 66–72.

[33] A. Fakhry, H. Cachet, C. Debiemme-Chouvy, Electrochim. Acta 179 (2015) 297−303.

[34] A. Fakhry, F. Pillier, C. Debiemme-Chouvy, J. Mater. Chem. A 2 (2014) 9859−9865.

[35] C. Debiemme-Chouvy, Electrochem. Commun. 11 (2009) 298-301.

[36] T. Darmanin, E.L. Klimareva, I. Schewtschenko, F. Guittard, I.F. Perepichka, Macromolecules 52 (2019) 8088–8102.

[37] T. Darmanin, F. Guittard, J. Mater. Chem. A 4 (2016) 3197–3203.

[38] C.R. Szczepanski, I. M'Jid, T. Darmanin, G. Godeau, F. Guittard, J. Mater. Chem. A 4 (2016) 17308–17323.

[39] S. Bai, Q. Hu, Q. Zeng, M. Wang, L. Wang, ACS Appl. Mater. Interfaces 10 (2018) 11319–11327.

[40] O. Sane, A. Diouf, G. Morán Cruz, F. Savina, R. Méallet-Renault, S. Amigoni, S.Y. Dieng, F. Guittard, T. Darmanin, Mater. Today 31 (2019) 119–120.

[41] O. Sane, A. Diouf, M. Pan, G. Morán Cruz, F. Savina, R. Méallet-Renault, S.Y. Dieng, S. Amigoni, F. Guittard, T. Darmanin, Electrochim. Acta 320 (2019) 134594.

[42] O. Thiam, A. Diouf, D. Diouf, S.Y. Dieng, F. Guittard, T. Darmanin, Phil. Trans. R. Soc. A 377 (2019) 20190123.

[43] G. Buemi, Bull. Chem. Soc. Jpn. 62 (1989) 1262–1268.

[44] V.S. Saji, K. K. Zong, M. Pyo, J. Photochem. Photobiol. A: Chem. 212 (2010) 81–87.

[45] Y. Wada, Y. Asada, T. Ikai, K. Maeda, T. Kuwabara, K. Takahashi, S. Kanoh, Chem. Select 1 (2016) 703–709.

[46] A.B.D. Cassie, S. Baxter, Trans. Faraday Soc. 40 (1944) 546–551.

[47] J. Ju, H. Bai, Y. Zheng, T. Zhao, R. Fang, L. Jiang, Nat. Commun. 3 (2012) 1247.

[48] L. Qu, L. Dai, M. Stone, Z. Xia, Z.L. Wang, Science 322 (2008) 238–242.

[49] L. Qu, L. Dai, Adv. Mater. 19 (2007) 3844–3849.

[50] M. Ge, C. Cao, J. Huang, X. Zhang, Y. Tang, X. Zhou, K. Zhang, Z. Chen, Y. Lai, Nanoscale Horiz. 3 (2018) 235–260.

[51] X. Dong, S. Gao, J. Huang, S. Li, T. Zhu, Y. Cheng, Y. Zhao, Z. Chen, Y. Lai, J. Mater. Chem. A 7 (2019) 2122–2128.

Graphical Abstract